Metrol. Meas. Syst., Vol. 31 (2024), No. 3
DOI: 10.24425/mms.2024.150287

METROLOGY AND MEASUREMENT SYSTEMS
Index 330930, ISSN 0860-8229
www.metrology.wat.edu.pl

FITTING METHOD OF SPINNING PROJECTILE TRI-ORTHOGONAL GEOMAGNETIC OUTPUT BASED ON IMPROVED PARTICLE SWARM OPTIMIZATION ALGORITHM

Zilu He[1)], Yiji Liu[1)], Qi Liang[1)], Yundong He[1)], Xin Chen[1)], Xiongzhu Bu[2)], Miaomiao Xu[3)]

1) *Shanghai Electro-Mechanical Engineering Institute, Shanghai, China*
2) *Nanjing University of Science and Technology, School of Mechanical Engineering, Nanjing, China* (✉ *buxu105@njust.edu.cn*)
3) *Nantong University, School of Information Science and Technology, Nantong, China*

Abstract

Obtaining the characteristics at a characteristic point of the outputs is a key step to the geomagnetic attitude measurement method of the spinning projectile. However, the actual outputs usually have some noise that cause the characteristic points to deviate from the theoretical position or produce multiple fake characteristic points, resulting in the increase of solution error and even the failure of solution. In addition, the coning motion and inaccurate initial alignment of the spinning projectile increase the number of unknown parameters and the computational complexity. In this study, several improved particle swarm optimization strategies are proposed. The actual outputs are fitted to the geomagnetic output equations under the coning motion, and the supervised learning effect of each strategy is analyzed and compared. The algorithm can be flexibly adjusted according to different needs in actual use by selecting appropriate strategies, which has wide applicability in data fitting.

Keywords: improved particle swarm optimization, geomagnetic attitude measurement, coarse initial parameter, weak boundary condition.

1. Introduction

Due to its high-speed rotation, the spinning projectile has high stability during flight and has become a widely used conventional weapon. In order to improve the hit accuracy of the spinning projectile fired by conventional artillery, many researchers have carried out researches on its attitude measurement method. With the development of MEMS magnetic sensors, the geomagnetic attitude measurement method has the advantages of miniaturization, low cost and low power consumption on the basis of meeting the requirements of all-time and all-weather autonomous attitude measurement, and has become one of the rapidly developed attitude measurement methods in recent years. However, the three output equations of the tri-orthogonal magnetic sensor are not independent of each other, it is unable to solve the full attitude angles. It can only be used as an auxiliary method to integrate with other attitude measurement methods such as inertial attitude measurement, infrared attitude measurement and so on [1-2]. In order to overcome this problem, some scientific researchers design algorithms which can independently solve the full attitude angles of the spinning projectile through the characteristics of the geomagnetic outputs, such as the zero-crossing method [3], the cross-ratio method [4], the integral ratio method [5], and the derivative ratio method [6]. However, most of these algorithms are based on the ideal state that the noise is very low. In this case, key parameters such as frequency and amplitude can be easily obtained according to the statistical regularity of noise and simple data processing such as FFT. Moreover, in most of these algorithms, the forward direction of the spinning projectile is regarded as always consistent with the tangent

Article history: received November 13, 2023; revised April 12, 2024; accepted May 5, 2024; available online June 24, 2024.

direction of the trajectory, and the coning motion of the spinning projectile due to the Magnus effect is ignored [7-9]. As a result, it is difficult to estimate the coning motion frequency and taper angle of the spinning projectile by traditional data processing methods. In addition, in practical applications, sometimes the initial state of the spinning projectile can only be obtained through rough alignment, so it is more difficult to estimate the geomagnetic output parameters. Therefore, it is necessary to propose a method that can accurately obtain the initial attitude angles, taper angle, spinning speed and coning motion frequency of the spinning projectile at the same time, so as to provide signal characteristics for the geomagnetic measurement method of the spinning projectile.

In view of the key parameters of the geomagnetic field and the motion characteristics of the spinning projectile, Li *et al.* established the attitude measurement model of the three-axis magnetic sensor of the spinning projectile [10]. On this basis, He *et al.* established the geomagnetic measurement model of spinning projectile under coning motion [6], providing a standard for calibrating geomagnetic characteristic parameters through data fitting. The actual output signals will inevitably be mixed with a certain degree of noise, which will affect the result of data fitting. In the calibration of magnetic sensors, Yu *et al.* calibrated AC vector magnetometer by ellipse fitting method [11]. Li *et al.* designed a least squares regression algorithm that can realize online calibration [12]. Sun *et al.* studied the error compensation method of ellipse fitting calibration magnetometer [13]. Li *et al.* proposed a dual inner product method to improve the calibration and alignment of the magnetometer [14]. Farhangian *et al.* fused the data of multiple magnetic sensors through UKF to accurately estimate the calibration parameters [15]. Crissidis *et al.* realized the calibration of magnetometers static errors with different dimensions based on the total least squares method [16]. The methods in Ref. [11-16] calibrate the magnetic sensor to eliminate static and dynamic errors, enabling the sensors to output more accurate signals. However, when solving the attitude angles using tri-orthogonal geomagnetic model, the geomagnetic signals will inevitably be coupled with noise. In order to eliminate the influence of noise, it is necessary to select appropriate optimization algorithms for processing geomagnetic signals.

Lu applied the gradient descent method to the inertial/geomagnetic navigation system and obtained the magnetic distortion parameters [17]. Zhou *et al.* adopted an improved iterative Gauss-Newton method to identify the aerodynamic parameters of high-spinning projectiles using GPS and geomagnetic measurement data [18]. Deng *et al.* introduced *backpropagation* (BP) neural networks to solve the inertial/geomagnetic attitude coupling model, reducing the root mean square error of attitude by more than 50% [19]. Cuenca *et al.* identified and described important contributors to the total magnetic field through deep learning and Gaussian regression processes to combat interference and noise [20]. Among the above optimization algorithms, the gradient descent method has slow convergence speed, poor stability, and is highly sensitive to initial conditions. The Gauss-Newton method may generate ill conditioned matrices during the solving process, resulting in incorrect results. The BP algorithm and deep learning can achieve high-precision results when there is a large amount of data available for learning. However, the flight time of conventional spinning projectile is limited. The amount of data is not enough and there are many parameters to be estimated. Therefore, a relatively simple algorithm is needed to obtain all the required attitude measurement model parameters.

2. Measurement model of tri-orthogonal magnetic sensor

The principle of the tri-orthogonal geomagnetic attitude measurement method of the spinning projectile is to obtain one of the attitude angles according to some characteristics at a certain position of the magnetic outputs. The other two attitude angles are solved by using the

tri-orthogonal geomagnetic equations. Ref. [6] provides the tri-orthogonal geomagnetic equations, as shown in (1) and (2)

$$\begin{cases} M_{sx0} = M_H \cos\psi_0 \cos\theta_0 - M_V \cos\psi_0 \sin\theta_0 \\ M_{sy0} = M_H(\sin\gamma_0 \sin\theta_0 - \cos\gamma_0 \sin\psi_0 \cos\theta_0) + M_V(\sin\gamma_0 \cos\theta_0 + \cos\gamma_0 \sin\psi_0 \sin\theta_0) \\ M_{sz0} = M_H(\cos\gamma_0 \sin\theta_0 + \sin\gamma_0 \sin\psi_0 \cos\theta_0) + M_V(\cos\gamma_0 \cos\theta_0 - \sin\gamma_0 \sin\psi_0 \sin\theta_0) \end{cases} \quad (1)$$

where M_H, M_V denote the horizontal and vertical component of the geomagnetic field vector norm, M_{sx0}, M_{sy0}, and M_{sz0} denote the outputs of the magnetic sensor without coning motion, and ψ_0, θ_0, and γ_0 are the magnetic yaw angle, magnetic pitch angle, and roll angle without coning motion, respectively. Within the range of conventional artillery, the variation of the geomagnetic field vector norm and magnetic declination are quite small, so M_H and M_V can be regarded as constants. When the spinning projectile flies in coning motion, the attitude angles need to be corrected by (2)

$$\begin{cases} \psi = \psi_0 + \delta \sin 2\pi f t \\ \theta = \theta_0 + \delta \cos 2\pi f t \\ \gamma = \gamma_0 \end{cases} \quad (2)$$

where ψ, θ, and γ denote the yaw angle, pitch angle, and roll angle with coning motion, δ is the taper angle, and f is coning motion frequency, respectively.

The tri-orthogonal geomagnetic attitude measurement method of spinning projectile includes cross ratio method, integral ratio method, derivative ratio method and so on. The characteristics of magnetic sensor outputs selected by these methods are different, as shown in Table 1.

Table 1. Characteristics required by tri-orthogonal geomagnetic attitude measurement method.

Measurement Method	**Characteristics**
Cross Ratio Method	Ratio between the Intersections of Outputs of y and z Axes and the Output of x Axis
Integral Ratio Method	Integration between 0-value Points of Outputs of y and z Axes
Derivative Ratio Method	Derivative at 0-value Points of Outputs of y and z Axes

However, when there is large interference in the output signals, no matter which algorithm is used, there will be two problems. The first is that the position of characteristic points will be offset due to noise, and the second is that the solution error of characteristics will be generated due to noise, as shown in Fig. 1.

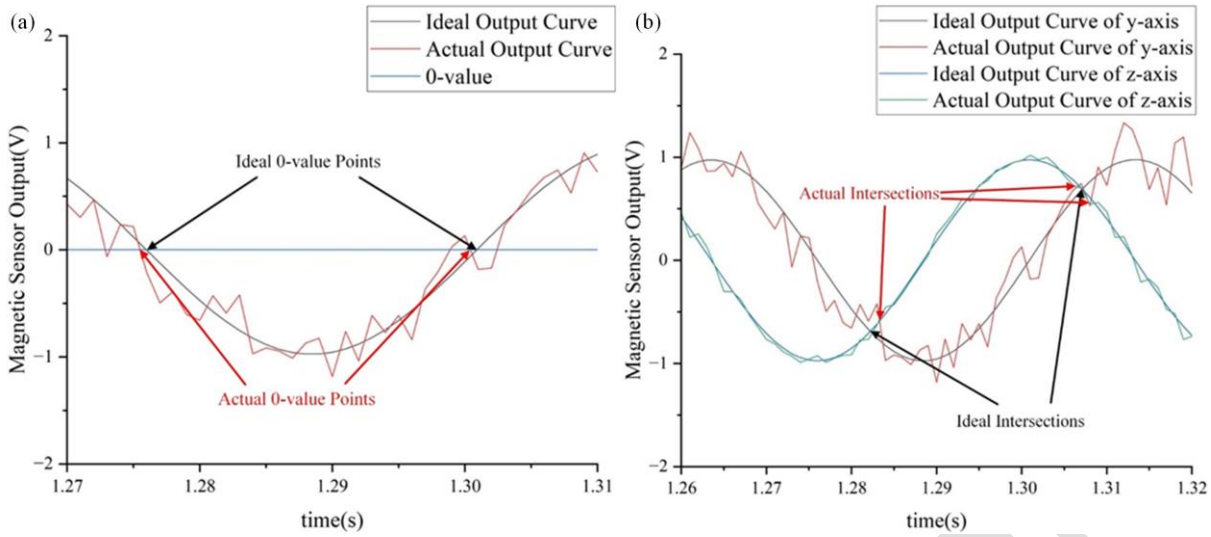

Fig. 1. Influence of noise on characteristic points with influence of noise on 0-value position (a) or influence of noise on intersection position (b).

In order to reduce the influence of noise on the tri-orthogonal geomagnetic attitude measurement method, the actual output signals of the magnetic sensor can be fitted to the standard output signals based on the tri-orthogonal geomagnetic equations. In this case, not only the position of characteristic points can be obtained quickly and directly by fitting the signals, but also the characteristic values can be directly calculated according to the fitted parameters, completely omitting the complex signal processing such as denoising and filtering.

3. Improved particle swarm optimization fitting algorithm

Particle swarm optimization (PSO) is an optimization algorithm with many advantages, such as simple steps, less parameters and fast convergence. In this study, an improved PSO algorithm is used to transform the problem of data fitting into a problem of nonlinear function optimization, and the results can be obtained simply and quickly through an indirect way.

Each particle in the PSO algorithm is a D dimension vector, which is a search individual in the optimization space. The particle position in each iteration can be regarded as a candidate solution, and the flight process of the particle is the search process. The particle speed can be adjusted in real time based on the optimal position of a single particle and all particles in the iterative process. A particle has only two attributes: speed and position. Speed represents the velocity of particle motion, and position represents the direction of particle optimization. The optimal solution in the optimization process of a single particle is the individual extreme value, and the optimal solution in the optimization process of all particles is the current global optimal solution. In each iteration, the particle speed, position and optimal solution are continuously updated, and the optimal solution is obtained when the convergence is finally completed or the termination condition is met [21-25]. The steps of PSO algorithm are as follows:

1) Initialize

First, set the termination condition. The maximum number of iterations is usually selected based on experience. Take initial condition randomly in the speed range and search space, and set the number of argument of the objective function, particle speed range $[V_{\min}, V_{\max}]$, position range $[x_{\min}, x_{\max}]$ and particle number N.

2) Individual extremum and global optimal solution

Define the fitness function and the selection principle of the optimal solution. The global optimal solution obtained in each iteration needs to be updated after comparing with the historical global optimal solution.

3) Update speed and position

Among the *N* particles in the *D* dimension space, the position and speed of the *i*th particle are expressed as $x_i = [x_{i1}, x_{i2}, \ldots, x_{id}]$ and $V_i = [V_{i1}, V_{i2}, \ldots, V_{id}]$, respectively. Update the speed and position according to (3) and (4)

$$V_{id}(k+1) = \omega V_{id}(k) + C_1 r_1 (P_{id}(k) - x_{id}(k)) + C_2 r_2 (G_{id}(k) - x_{id}(k)) \tag{3}$$

$$x_{id}(k+1) = x_{id}(k) + V_{id}(k+1) \tag{4}$$

where, $i = 1, 2, \cdots, N$, $d = 1, 2, \cdots, D$, ω is the inertia weight factor, which is usually a constant in the conventional PSO algorithm. k is the current iteration number. C_1 and C_2 are learning factors, generally 2. r_1 and r_2 are random numbers evenly distributed between 0 and 1. $P_{id}(k)$ and $G_{id}(k)$ are the fitness and global fitness of the *i*th particle, respectively.

During fitting, the fitness function can be constructed by the least square method, and the problem can be converted into the optimization problem of obtaining the minimum value of the function, as shown in (5).

$$M_i = \min\left[\sqrt{(\boldsymbol{M}_\mathrm{s} - \boldsymbol{M}_\mathrm{t})^\mathrm{T} (\boldsymbol{M}_\mathrm{s} - \boldsymbol{M}_\mathrm{t})}\right] \tag{5}$$

where, M_i is the fitness, $\boldsymbol{M}_\mathrm{t}$ is the actual outputs of the magnetic sensor, and $\boldsymbol{M}_\mathrm{s}$ is the ideal outputs of the magnetic sensor.

Combining (1) and (2), the estimated parameters of the attitude measurement outputs of the spinning projectile are initial attitude angles $\psi_\mathrm{i} = \psi(0)$, $\theta_\mathrm{i} = \theta(0)$, $\gamma_\mathrm{i} = \gamma(0)$, taper angle δ and coning motion frequency f. The initial roll angle is defined manually, and is usually taken as 0 for convenience. In addition, replace the roll angle γ with a function of time $\gamma = 2\pi f_0 t$, where f_0 is the roll angle frequency. Then there are 5 parameters to be estimated of this question, namely ψ_0, θ_0, f_0, δ, f.

In the actual situation, all physical quantities have initial values and constraints. When fitting the tri-orthogonal magnetic sensor attitude measurement outputs, the constraint conditions should be set according to (6).

$$\begin{cases} 0 \le \psi_\mathrm{l} < \psi_\mathrm{i} < \psi_\mathrm{h} < 2\pi \\ -\pi/2 \le \theta_\mathrm{l} < \theta_\mathrm{i} < \theta_\mathrm{h} \le \pi/2 \\ f_0 > 0 \\ \delta > 0 \\ f > 0 \end{cases} \tag{6}$$

where ψ_h, ψ_l are the upper and lower limit of magnetic yaw angle coarse alignment, θ_h, θ_l are the upper and lower limit of magnetic pitch angle coarse alignment. According to the stability theory of spinning projectile, the roll angle frequency of spinning projectile is proportional to the coning motion frequency, which is related to the length-diameter ratio of

projectile, and the proportion is m. As an important structural parameter of the projectile, the length-diameter ratio of the projectile is a known quantity. Assuming that the proportion range estimated by the projectile length-diameter ratio is $m_{\mathrm{l}} \sim m_{\mathrm{h}}$, (6) can be upgraded to (7).

$$\begin{cases} 0 \le \psi_{\mathrm{l}} < \psi_{\mathrm{i}} < \psi_{\mathrm{h}} < 2\pi \\ -\pi/2 \le \theta_{\mathrm{l}} < \theta_{\mathrm{i}} < \theta_{\mathrm{h}} \le \pi/2 \\ 0 < f/m_{\mathrm{h}} < f_0 < f/m_{\mathrm{l}} \\ \delta > 0 \\ f > 0 \end{cases} \tag{7}$$

In PSO, inertia weight factor ω is a parameter that affects the exploration ability of the algorithm. The value is higher, the global search ability is stronger. The value is smaller, the local search ability is stronger. Because the strong nonlinearity of the tri-orthogonal magnetic sensor outputs, the fitness function constructed by (5) have a lot of local optimal values. This raises problems such as spending too long time to search for the optimal value, easy to fall into the local optimum, and unable to select the optimal value. In order to give consideration to the global and local search ability of the algorithm, the inertia weight factor should be gradually reduced during the whole optimization process, so that the iterative process can quickly converge to the interval of the optimal solution.

The adaptive adjustment strategy is used to dynamically adjust the inertia weight of particles, which can make the inertia weight of particles take a larger value in the early stage and improve the activity of particles. On the contrary, the weight can be reduced in the later stage, so that the particles can converge near the elite particles and close to the global optimal solution. For convenience, the following strategies can be used to adjust the weights.

(1) Reduce by the linear function
(2) Reduce by the concave quadratic function
(3) Reduce by the convex quadratic function
(4) Reduce by the tangent function
(5) Reduce by the arctangent function

4. Experiment and results

The experimental equipment in Ref. [6] is used to verify the improved PSO algorithm proposed in this study, as shown in Fig. 2.

Fig. 2. Semi-physical experimental device.

Adjust the turntable so that it can carry the semi-physical device to make coning motion according to the following parameters.

$$\begin{cases} \psi_{\mathrm{i}}=30° \\ \theta_{\mathrm{i}}=80° \\ f_0=20\mathrm{Hz} \\ \delta=5° \\ f=2\mathrm{Hz} \end{cases} \tag{8}$$

According to (1), the outputs of y-axis and z-axis magnetic sensors are affected by more parameters to be estimated, and the outputs of y-axis and z-axis are only different in phase. Therefore, the output of y-axis is taken as an example, and its actual measured normalized output is shown in Fig. 3.

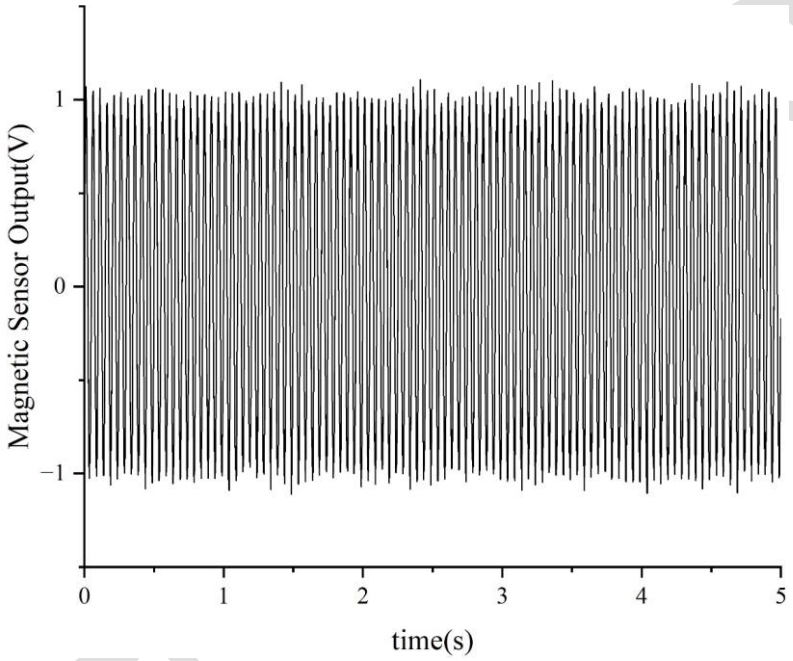

Fig. 3. Actual output curve of y-axis.

From Fig. 3, it can be found that the information about the size of taper angle and the coning motion frequency has almost disappeared in the noise.

Then the constraints should be set. In other commonly used attitude measurement methods, such as inertial attitude measurement, it is necessary to obtain more accurate initial states through initial alignment. However, the fitting method proposed in Section 3 of this study does not need such accurate initial states. The initial state values can be set in a quite large range, even can be directly determined by the naked eye. In addition, assuming $m=10\pm0.4$, the fitting constraints are shown in (9).

$$\begin{cases} 0°<\psi_{\mathrm{i}}<45° \\ 45°<\theta_{\mathrm{i}}<180° \\ f_0>0 \\ \delta>0 \\ 0<f_0/10.4<f<f_0/9.6 \end{cases} \tag{9}$$

The commonly used fixed weight and linear weight reduction strategies in PSO algorithm, and four improved weight strategies are adopted to solve the fitness function. The maximum number of iterations is set to 300, the number of particles is 1000, the fixed weight factor is set to 0.2, and the weight of improved methods are reduced from 0.8 to 0.2 according to their respective function rules.

$$\begin{cases} \omega_1 = 0.2 \\ \omega_2 = 0.8 - 0.002k \\ \omega_3 = -\dfrac{3k^2}{449995} + \dfrac{359999}{449995} \\ \omega_4 = \dfrac{3k^2}{447005} - \dfrac{360k}{89401} + \dfrac{359401}{447005} \\ \omega_5 = \dfrac{-3\tan[8(k-149.5)\pi/2700]}{10\tan(4\pi/9)} + 0.5 \\ \omega_6 = -\dfrac{3\arctan[(k-149.5)/3]}{5\pi} + 0.5 \end{cases} \tag{10}$$

where k is the number of iterations.

Figure 4 shows the weight changes of different improved strategies.

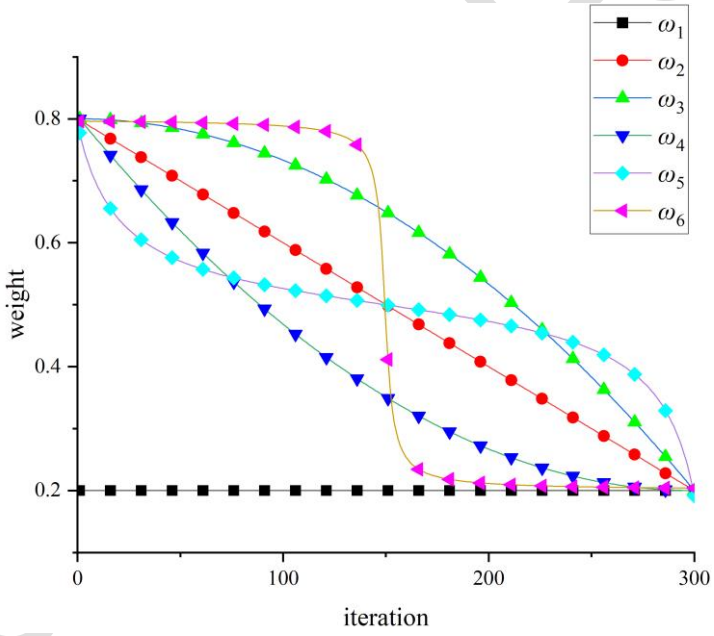

Fig. 4. Schematic diagram of weight change.

The semi-physical device records the data measured by sensors during the motion process and performs fitting calculations offline. The fitting results are shown in Table 2 to Table 7, and the solution that do not get the global optimum are marked with "*". After multiple iterations in each fitting test, the fitted parameters will converge to a fixed value, and the convergence position in the tables is the number of iterations at convergence. To compare the fitting effects of different weight optimization strategies, the same dataset is used for fitting.

Table 2. Fitting results of fixed weight factor.

Fitting times	ψ_i(°)	θ_i(°)	f_0(Hz)	δ(°)	f(Hz)	Convergence position
1	29.9703	80.0966	19.9999	5.3176	2.0002	39
2	29.4504	79.2840	20.0002	4.9184	1.9969	93
3	29.9278	80.1011	20.0000	5.0534	1.9991	37
4	29.9008	80.2412	19.9999	5.1431	2.0001	143
5*	39.2365	82.0403	20.0000	2.1255	2.0682	239
6*	0	99.5424	19.9958	3.1294	2.0678	35
7	30.3216	79.8315	20.0001	4.9652	2.0008	47
8*	45.0000	82.5914	20.0003	4.0088	2.0065	70
9	29.3786	79.9269	20.0000	5.1204	2.0005	28
10*	0	99.6112	19.9959	3.7521	2.0678	50

Table 3. Fitting results of linear weight factor.

Fitting times	ψ_i(°)	θ_i(°)	f_0(Hz)	δ(°)	f(Hz)	Convergence position
1	29.5875	79.9849	19.9999	4.9389	1.9992	243
2*	0	99.4254	19.9958	3.1856	2.0678	121
3*	45.0001	82.4429	20.0003	3.7128	2.0090	171
4	28.6651	79.4177	20.0000	5.0649	1.9981	269
5	30.1441	80.0197	20.0001	4.9111	2.0000	155
6	29.1025	79.9667	19.9999	5.0345	1.9991	184
7	30.1184	79.9681	20.0001	4.7954	2.0012	132
8	30.1239	79.9584	20.0000	5.0877	2.0022	124
9	30.5661	80.1467	19.9999	5.0952	2.0020	227
10	25.6855	78.7299	19.9999	5.1224	2.0018	285

Table 4. Fitting results of concave quadratic weight factor.

Fitting times	ψ_i(°)	θ_i(°)	f_0(Hz)	δ(°)	f(Hz)	Convergence position
1	30.4185	79.9689	20.0000	4.9205	1.9995	272
2	29.7814	80.0028	20.0000	4.8883	2.0019	195
3	29.6732	79.7825	20.0001	5.0264	2.0011	284
4	30.5923	80.2041	20.0000	5.0006	2.0017	265
5*	0.0000	99.2765	19.9959	3.2757	2.0678	195
6	30.5432	79.8731	20.0001	5.0275	2.0025	235
7	31.5388	80.4662	20.0000	4.8013	2.0039	265
8*	0.0000	80.0772	19.9959	0.0000	2.0623	290
9	31.5860	80.1365	20.0002	4.7041	2.0009	231
10	29.7223	79.9971	19.9999	5.1213	2.0000	243

Table 5. Fitting results of convex quadratic weight factor.

Fitting times	ψ_i(°)	θ_i(°)	f_0(Hz)	δ(°)	f(Hz)	Convergence position
1*	0.0000	80.0291	19.9959	7.0361	1.9489	291
2	31.9462	80.4688	20.0000	4.9832	2.0019	211
3	29.0827	80.0553	19.9999	4.9563	1.9983	110
4	31.6281	80.1762	20.0001	4.9812	2.0034	153
5	28.9830	79.5413	20.0000	4.8768	1.9968	141
6*	0.0000	100.0791	19.9958	3.0577	2.0678	84
7	30.8577	80.1553	20.0000	4.9351	1.9993	158
8	29.9823	79.8880	20.0000	5.0567	1.9983	172
9	29.7722	79.9363	19.9999	5.1987	1.9979	138
10	30.5448	79.9819	20.0001	4.9716	2.0002	189

Table 6. Fitting results of tangent weight factor.

Fitting times	ψ_i(°)	θ_i(°)	f_0(Hz)	δ(°)	f(Hz)	Convergence position
1	24.4093	81.3644	19.9988	5.0721	2.0403	81
2	31.3757	80.4418	20.0001	4.8237	2.0003	94
3*	43.4362	82.5611	20.0001	3.9973	2.0089	83
4	32.2897	80.9197	19.9999	5.0543	1.9976	98
5	31.1643	80.2741	20.0000	4.9964	1.9990	106
6	29.9912	79.6465	20.0002	5.0349	2.0014	130
7	31.1679	81.1749	19.9996	4.9057	2.0036	93
8	30.7873	79.8559	20.0002	4.7361	2.0010	87
9	31.6597	80.3501	20.0001	5.0828	2.0019	93
10	28.8787	79.7702	19.9999	5.3184	2.0003	120

Table 7. Fitting results of arctangent weight factor.

Fitting times	ψ_i(°)	θ_i(°)	f_0(Hz)	δ(°)	f(Hz)	Convergence position
1	29.7243	79.8972	20.0001	5.0384	1.9984	198
2	29.6049	79.7290	20.0001	5.0981	2.0007	220
3	31.3681	80.2188	20.0002	4.8864	1.9994	177
4	30.6718	79.9434	20.0001	4.8412	2.0007	179
5	30.0270	80.0158	19.9999	4.9662	1.9998	223
6	30.7264	79.8772	20.0001	4.9464	2.0011	179
7	30.7567	80.0707	20.0001	4.9888	1.9997	189
8	30.4703	80.0085	20.0000	4.7779	1.9970	185
9	30.9410	80.4645	19.9999	5.1159	2.0014	187
10	31.0908	80.4559	19.9999	5.1015	2.0019	214

The differential evolution algorithm exhibits strong robustness in solving non convex, multimodal, and nonlinear function optimization problems, especially adept at handling multivariate function optimization problems. So, differential evolution algorithm with adaptive mutation operator is selected to compare with the proposed improved PSO algorithm.

Table 8. Fitting results of differential evolution algorithm with adaptive mutation operator.

Fitting times	ψ_i(°)	θ_i(°)	f_0(Hz)	δ(°)	f(Hz)
1	31.8335	81.3199	19.9994	4.0222	2.0261
2	35.4177	81.6571	20.0002	4.7767	2.0055
3	26.0483	78.8646	19.9998	5.7468	1.9785
4	22.5028	77.1077	20.0002	5.1273	1.9740
5	31.2693	77.3764	20.0019	2.7498	1.9970
6	24.8903	77.6863	20.0002	5.2514	1.9944
7	21.0085	75.5578	19.9992	4.5625	1.9772
8	31.9449	80.8591	19.9998	4.8565	1.9994
9	41.4907	82.6164	19.9999	4.3217	2.0048
10	33.6637	83.4166	19.9982	3.3272	2.0102

5. Discussion

It can be seen from the fitting data that the PSO algorithm and its improved algorithms have relatively good fitting effect under the condition of uncertain initial state and loose constraints. Because the particles move randomly, the convergence position of some data are far from the convergence position of other data in the same group, but most of them are close to each other. The PSO algorithm can converge to a local optimum at a fast speed due to its small weight

factor, but it is difficult to ensure that the point is the global optimum, so there is a high probability that accurate fitting results cannot be obtained. The convex quadratic improved algorithm and the tangent improved algorithm have a fast rate of inertia weight factor reduction in the early stage, so they converge fast. The tangent improved algorithm has a long time to maintain at the middle weight, so the fitting results are more stable than the convex quadratic improved algorithm. The other three improved algorithms search the global optimum in the early stage. They convergence slowly because of the slow reduction of inertia weight factor. Among all of the improved algorithms, the tangent improved algorithm has fast speed and relatively good stability, while the arctangent improved algorithm has the highest stability. These two algorithms have high application value under loose constraints, but also have the disadvantage of complex calculation of inertia weight factor reduction function. Other improved algorithms can easily determine the inertia weight factor reduction function, and can also improve their fitting stability when the initial states are relatively accurate.

Compared to differential evolution algorithm with adaptive mutation operator, the improved PSO algorithm has higher accuracy. This is because differential evolution algorithm may have low solving accuracy when the complexity of the problem to be solved is high. In addition, the differential evolution algorithm needs to set upper and lower limits for each parameter to be solved, which is equivalent to strengthening constraints compared to the proposed algorithm. Therefore, the improving PSO algorithm has more advantages in solving similar problems.

6. Conclusions

Because it is difficult to determine the position of the characteristic points and the solution results are biased greatly when the characteristics are obtained from the measured outputs of the magnetic sensor under the coning motion directly, an improved PSO algorithm to get the approximate standard outputs by data fitting is proposed in this study. By comparing different improved strategies, the advantages, disadvantages and applicability of each strategy are analyzed. This method can get quite accurate estimated parameters under loose constraints and initial conditions. It can provide a stable and accurate supervised learning algorithm in a wide range of similar applications.

Compared to the rate of change in roll angle and the rate of change in pitch angle and yaw angle caused by coning motion, the rate of change in pitch angle caused by trajectory is much smaller. Therefore, in current tri-orthogonal geomagnetic attitude measurement model, the pitch angle centre value is considered constant in a single calculation. The pitch angle obtained from each solution is treated as the initial condition for the next iteration. The attitude solution model should update if the trajectory model is known and this will bring more undetermined parameters and constraints. Because the significant computational resources required for improved PSO algorithm, upgrading the attitude measurement model may lead to overfitting and require more computation time. In subsequent research, further consideration should be given to improving the fitting strategy of improved PSO algorithm, so it can have better fitting efficiency and effect for more complex models.

Acknowledgements

This work was supported by the National Natural Science Foundation of China [61675097] and [62101287].

References

[1] He, Z., Bu, X., Yang, H., & Song, Y. (2021). Interacting multiple model cubature Kalman filter for geomagnetic/infrared projectile attitude measurement. *Measurement*, *174*(1), 109077. https://doi.org/10.1016/j.measurement.2021.109077

[2] Wang, W., Meng, G., Liu, J., Wang, M., Gao, Z., Mu, L., & Zhang, S. (2018, December). *Integrated navigation method based on inertial and geomagnetic information fusion. In Optical Sensing and Imaging Technologies and Applications* (Vol. 10846, pp. 278-292). SPIE. https://doi.org/10.1117/12.2504356

[3] Xiang, C., Bu, X. Z., & Yang, B. (2014). Three different attitude measurements of spinning projectile based on magnetic sensors. *Measurement*, *47*, 331-340. https://doi.org/10.1016/j.measurement.2013.09.002

[4] Yu, J., Bu, X., Xiang, C., & Yang, B. (2017). Spinning projectile's attitude measurement using intersection ratio of magnetic sensors. Proceedings of the Institution of Mechanical Engineers, *Part G: Journal of Aerospace Engineering*, *231*(5), 866-876. https://doi.org/10.1177/0954410016644628

[5] Xu, M., Bu, X., He, Z., & Han, W. (2019). Integral ratio method for the geomagnetic attitude measurement of spinning projectiles. *Journal of Harbin Engineering University*, *40*(06), 1163-1168. https://doi.org/10.11990/jheu.201804009

[6] He, Z., Bu, X., Yang, H., & Song, Y. (2021). Derivative ratio attitude solution algorithm of tri-orthogonal magnetic sensor for spinning projectile. *Measurement*, *186*, 110228. https://doi.org/10.1016/j.measurement.2021.110228

[7] Chughtai, F. A., Masud, J., & Akhtar, S. (2019). Unsteady aerodynamics computation and investigation of magnus effect on computed trajectory of spinning projectile from subsonic to supersonic speeds. *The Aeronautical Journal*, *123*(1264), 863-889. https://doi.org/10.1017/aer.2019.32

[8] Lijin, J., & Jothi, T. J. S. (2018). Aerodynamic characteristics of an ogive-nose spinning projectile. *Sādhanā*, *43*, 1-8.

[9] Norris, J., Hameed, A., Economou, J., & Parker, S. (2020). A review of dual-spin projectile stability. *Defence Technology*, *16*, 1-9. https://doi.org/10.1016/j.dt.2019.06.003

[10] Li, D., & Bu, X. Z. (2010). Roll angle measurement of spinning projectile based on non-orthogonal magnetic sensors. *Acta Armamentarii*, *31*(10), 1316-1321.

[11] Yu, X., Xiao, C., Liu, S., Zong, Q., Qu, Y., Chen, H., Zou, H., Shi, W., Wang, Y., Chen, A., Song, S., Gao, S., & Shao, S. (2020). Calibration of AC vector magnetometer based on ellipsoid fitting. *IEEE Transactions on Instrumentation and Measurement*, *70*, 1-6. https://doi.org/10.1109/TIM.2020.3014980

[12] Li, L., & Huang, J. (2018). Recursive of Least Square Based Online Calibration Method in Geomagnetic Detection. *In MATEC Web of Conferences* (Vol. 232, p. 04087). EDP Sciences.

[13] Sun, W., Yang, Y. H., & Wang, Y. (2018). Research on Error Correction of Magnetometer Based on Ellipsoid Fitting [J]. *Chinese journal of sensors and actuators*, *31*(09), 1373-1376. https://doi.org/10.3969/j.issn.1004-1699.2018.09.013

[14] Li, X., Song, B., Wang, Y., Niu, J., & Li, Z. (2018). Calibration and alignment of tri-axial magnetometers for attitude determination. *IEEE Sensors Journal*, *18*(18), 7399-7406. https://doi.org/10.1109/JSEN.2018.2859832

[15] Farhangian, F., Bilel, S., Farhangian, F., & Landry Jr, R. (2021). A magnetometer calibration method using single-axis motion trajectory and unscented Kalman filter for body motion capture applications. *International Journal of Sensors and Sensor Networks*, *9*(1), 1. https://doi.org/10.11648/J.IJSSN.20210901.11

[16] Crassidis, J. L., & Cheng, Y. (2021). Three-axis magnetometer calibration using total least squares. *Journal of Guidance, Control, and Dynamics*, *44*(8), 1410-1424. https://doi.org/10.2514/1.G005305

[17] Lu, J. (2016). *A fault tolerant, data fusion system for navigation applications to a ducted fan VTOL UAV*. Open Access Master's Report, Michigan Technological University, 2016. https://doi.org/10.37099/mtu.dc.etdr/98

[18] Zhou, Z., Wang, L., Fu, J., & An, L. (2021, July). Aerodynamic parameters identification for high-spinning projectile based on geomagnetic data. *In 2021 40th Chinese Control Conference* (*CCC*) (pp. 1236-1242). IEEE. https://doi.org/10.23919/CCC52363.2021.9549442

[19] Deng, Z., Wang, J., Liang, X., & Liu, N. (2020). A coupling method of geomagnetic aided inertial attitude errors. *IEEE Sensors Journal*, *20*(23), 14282-14289. https://doi.org/10.1109/JSEN.2020.3007210

[20] Cuenca, A., & Moncayo, H. (2022). Machine learning application to estimation of magnetospheric contributions for geomagnetic-based navigation. *In AIAA SCITECH 2022 Forum* (p. 1714). https://doi.org/10.2514/6.2022-1714

[21] Wang, H., Jin, Y., & Doherty, J. (2017). Committee-based active learning for surrogate-assisted particle swarm optimization of expensive problems. *IEEE Transactions on Cybernetics*, *47*(9), 2664-2677. https://doi.org/10.1109/TCYB.2017.2710978

[22] Bui, D. T., Bui, Q. T., Nguyen, Q. P., Pradhan, B., Nampak, H., & Trinh, P. T. (2017). A hybrid artificial intelligence approach using GIS-based neural-fuzzy inference system and particle swarm optimization for forest fire susceptibility modeling at a tropical area. *Agricultural and forest meteorology*, *233*, 32-44. https://doi.org/10.1016/j.agrformet.2016.11.002

[23] Ding, Y., Cheng, L., Pedrycz, W., & Hao, K. (2015). Global nonlinear kernel prediction for large data set with a particle swarm-optimized interval support vector regression. *IEEE transactions on neural networks and learning systems*, *26*(10), 2521-2534. https://doi.org/10.1109/TNNLS.2015.2426182

[24] Su, Y. X., & Chi, R. (2017). Multi-objective particle swarm-differential evolution algorithm. *Neural Computing and Applications*, *28*, 407-418. https://doi.org/10.1007/s00521-015-2073-y

[25] Tang, B., Zhanxia, Z., & Luo, J. (2017). A convergence-guaranteed particle swarm optimization method for mobile robot global path planning. *Assembly Automation*, *37*(1), 114-129. https://doi.org/10.1108/AA-03-2016-024

Zilu He received his Bachelor and Master degrees in measurement& control technology and instrument and instrument engineering from NJUST in 2014 and 2017, respectively, and his PhD degree in instrument science and technology from NJUST in 2022. He is currently an engineer at Shanghai Electro-Mechanical Engineering Institute. His current research interest is dynamic measurement, signal processing and fault diagnosis.

Qi Liang received the MS degree in optical engineering from NJUST, China, in 2013. He is currently Senior Engineer with Shanghai Electro-Mechanical Engineering Institute. His current research interest is measurement system design.

Yiji Liu obtained his MS degree in management from University of Leicester, UK, in 2011. He is currently Senior Engineer with Shanghai Electro-Mechanical Engineering Institute. His research activity focuses on project management about measurement and control system design.

Xin Chen graduated from HIT, China, in 2012, majoring in communication and information system. He is currently Senior Engineer with Shanghai Electro-Mechanical Engineering Institute.His current research interest is telemetry system design.

Miaomiao Xu received his Bachelor and PhD degrees in instrument science and technology from NJUST, China in 2014 and 2019. He is currently an associate professor with the School of Information Science and Technology, Nantong University, China. His research interests are focused on signal processing, integrated navigation and instrumental science and technology.

Xiongzhu Bu is a professor at Nanjing University of Science and Technology (NJUST). He received his BS and MS degrees in dynamic measurement from NJUST in 1988 and 1990, respectively, and his PhD degree in dynamic measurement from NJUST in 1993. His current research interests include sensor technology, dynamic measurements, digital signal processing, smart instrumentation design and application.

Yundong He graduated from ECNU, China, in 2010, majoring in circuit and system. He is currently Senior Engineer with Shanghai Electro-Mechanical Engineering Institute. His current research interest is telemetry system design.